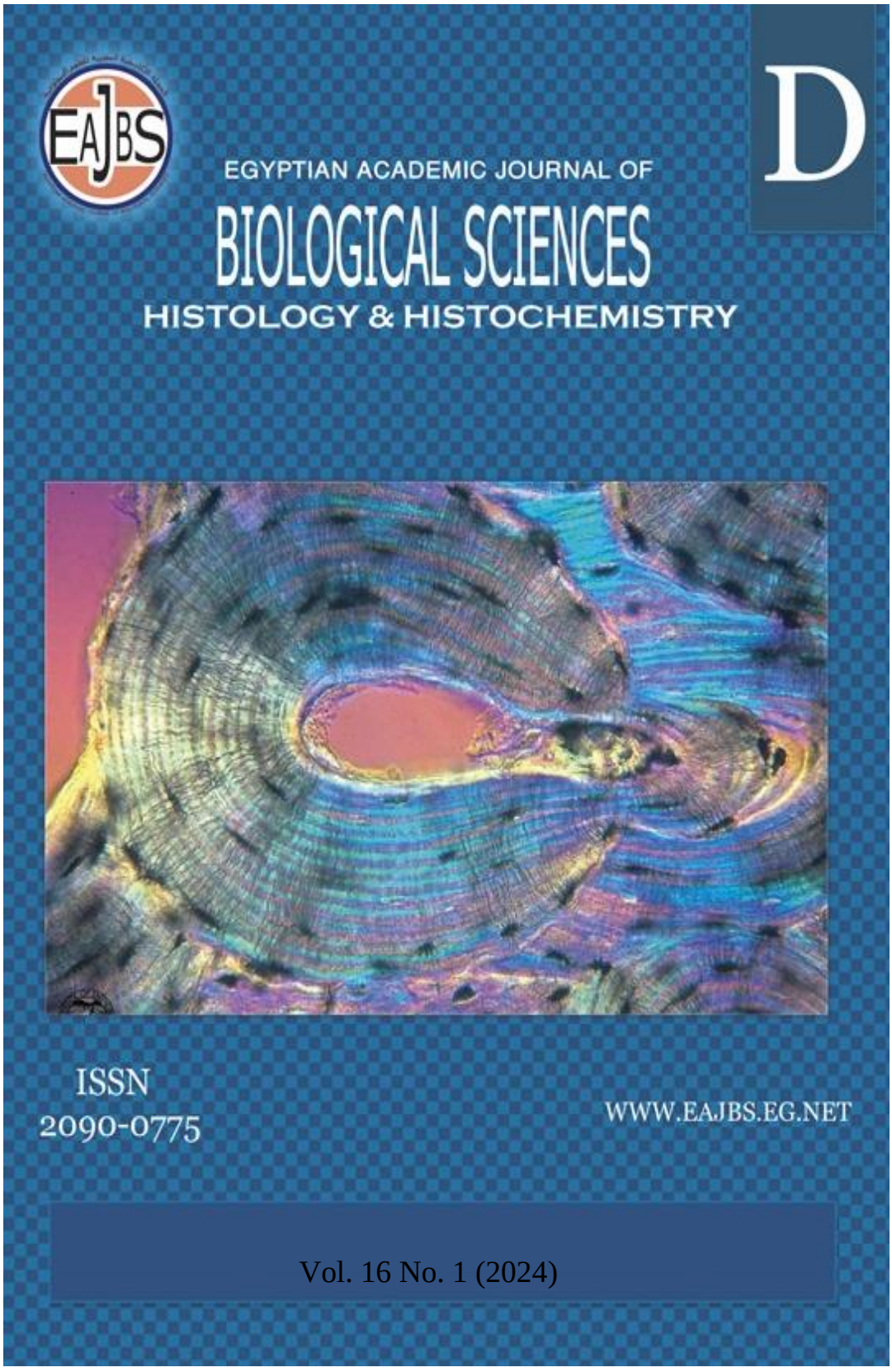

Citation: Egypt. *Acad. J. Biolog. Sci. (D-Histology and histochemistry) Vol.16(1) pp155-177(2024)*
DOI: 10.21608/EAJBSD.2024.355544

Egypt. Acad. J. Biolog. Sci., 16(1): 155-177 (2024)

Egyptian Academic Journal of Biological Sciences
D. Histology & Histochemistry
ISSN 2090 – 0775
http://eajbsd.journals.ekb.eg

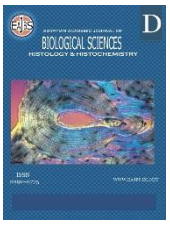

Effects of Maternal Diabetes on Prenatal Development of The Vertebral Column in The Albino Rat and Possible Protective Role of Arachidonic Acid

Ashraf E. Bastwrous[1]; Refaat S. Mohamed[1]; Ayman S. Amer[1&2] and Martha E. Adly[1]

[1]Department of Human Anatomy and Embryology, Faculty of Medicine, Assiut University, Assiut 71526, Egypt.

[2]Department of Biomedical Sciences, College of Medicine, King Faisal University, AlAhsa, Saudi Arabia.

***E-mail:** ashrafedward@aun.edu.eg - ayounis@kfu.edu.sa

ARTICLE INFO

Article History
Received:5/4/2024
Accepted:21/ 5/2024
Available:25/5/2024

***Keywords*:**
Diabetes, Vertebral Column, Arachidonic Acid.

ABSTRACT

Maternal diabetes is considered one of the most common causes of defective growth of the fetus. Polyunsaturated fatty acids (PUFAs) help prevent alloxan-induced type 1 diabetes mellitus (type 1 DM). It was found that arachidonic acid (AA) is the most successful PUFA in preventing rats from developing type 1 diabetes brought on by alloxan. The aim of this work is to investigate the effects of maternal diabetes on the prenatal development of rat vertebral columns and the probable protecting role of arachidonic acid. Randomly selected pregnant rats were divided into four groups: control, alloxan-induced diabetes group (150 mg/kg), alloxan + arachidonic acid group (55µg/kg, followed by alloxan injection), and arachidonic acid group (arachidonic acid only). The female pregnant rats were sacrificed at the gestational days 15, 17 and 19. The fetuses were collected and subjected to morphometric analysis. The lumbar vertebrae and the sacrum were removed and managed for light and electron microscopic examination. In the alloxan-induced diabetic group, the offspring exhibited a significant drop in all body measurements. Histologic examination of lumbar and sacral vertebrae in the offspring of the alloxan-induced diabetic group showed delayed chondrification and ossification. Electron microscopic examination of reserve cell of the alloxan-induced diabetic group of the 19-day-old albino rat fetus shows shrinkage of the cell with irregular outline and cytoplasmic vacuolations. In the alloxan + arachidonic acid group, the morphometric measurements of the offspring and the histological picture of their lumbar and sacral vertebrae were more or less similar to the control group.

INTRODUCTION

The vertebral column of the rat is composed of a number of vertebrae, subdivided into 7 cervical, 13 thoracic (all articulating with ribs), 6 lumbar, 4 sacral and caudal (tail) vertebrae ranging from 25 to 30 (Maynard and Downes, 2019).

Bone development starts prenatally during the fetal life (Zoetis *et al.*, 2003). At the end of the 9th day of rat embryonic life or at the beginning of the 10th day, somite development starts. The vertebral column arises from the sclerotome portions of adjacent somites. These sclerotome cells differentiate into fibroblasts and chondroblasts (Yilmaz and Tokpinar, 2019). The caudal region of one sclerotome joins with the superior region of the subjacent sclerotome.

The newly formed structure is composed of portions of two adjacent sclerotomes (DeSesso and Scialli, 2018). Then, mesenchymal vertebrae are chondrified at day 14 (Jones *et al.,* 1991; DeSesso and Scialli, 2018).

Ossification in the vertebral bodies starts around day 18 in the midthoracic region and from there, it proceeds in both cephalic and caudal directions. This ossification pattern shows how the neural tube's closure is progressing. (day 10-11) (Jones *et al.,* 1991; Burdan *et al.,* 2016). On day 20, each vertebra is formed by a cartilaginous or partially ossified ventral corpus, two lateral arches (usually ossified) and a cartilaginous dorsal neural spine (El-Nahla *et al.,* 2017).

Endochondral ossification is the process that results in longitudinal bone development. It begins when progenitor cells in the growth plate's resting zone are stimulated to proliferate and activated to become chondrocytes. At the growth plate hypertrophic zone, it proceeds through stages of maturation, hypertrophy, and apoptosis (Xian *et al.,* 2004). Through the epiphyseal plate, the bone lengthening is taking place. Bone growth is inhibited by damage to the plate (Maynard and Downes, 2019).

A chronic condition known as diabetes mellitus is defined by an absolute or relative insulin insufficiency, resulting in hyperglycemia. Chronic hyperglycemia can cause various complications such as nephropathy, neuropathy, retinopathy and increased risk of cardiovascular disease (Balaji *et al.,* 2020).

It is known that having diabetes during pregnancy causes abnormal growth in the fetus. The newborns of mothers with diabetes have reduced bone mineral content and hypoplasia of the forelimb, hindlimb, neurocranial, and viscerocranial bones. (Shamsi *et al.,* 2020). Studies on gestational diabetes show that the prevalence of congenital abnormalities increases despite greater clinical attempts to enhance glycemic control during diabetic pregnancy. (Eriksson and Wentzel, 2015).

Because alloxan is quickly absorbed by β-cells, it is a medication that can make animals develop diabetes-like symptoms. Hexokinase-induced alloxan reduction triggers a redox cycle that escalates the generation of reactive oxygen species (ROS) and results in β-cell necrosis (Szkudelski, 2001).

Polyunsaturated fatty acids (PUFAs) may prevent alloxan-induced type 1 diabetic mellitus (type 1 DM). It was found that arachidonic acid (AA) is the most successful PUFA in preventing rats from developing type 1 diabetes brought on by alloxan (Gundala *et al.,* 2018).

MATERIALS AND METHODS

Experimental Animals:

A total number of 40 adult female (3-month-olds weighing 150-200 gm) and 10 adult male (3-month-olds weighing 200-250 gm) albino rats were obtained from Animal House (Faculty of Medicine, Assiut University). The animals were kept in temperature-controlled environments in stainless steel cages with a 12:12 light/dark cycle. Food and water were freely available.

Experimental Protocol:

Female rats were randomly divided into 4 groups:

1-Control group: (10) rats, received no treatment.

2-Experimental group (a) (Alloxan group): (10) rats. Diabetes was induced in this group by an intraperitoneal single injection of alloxan monohydrate (obtained from Alpha Chem Company) dissolved in a normal saline solution (150 mg/kg body weight). The diagnosis of diabetes was evaluated by measuring blood glucose levels 72 hours and 1 week following alloxan injection. The On Call Plus blood glucose monitor was used to measure blood glucose. The study's rats were then chosen based on their blood glucose levels exceeding 200 mg/dl. (Saleh *et al.,* 2017).

3-Experimental group (b) (Alloxan + Arachidonic acid group): (10) rats,

were given AA (obtained from Santa Cruz Company) at a dose of 55µg/kg orally daily for a week followed by an intraperitoneal single injection of alloxan monohydrate and then AA was given once in a week for the whole duration of the study (Gundala *et al.,* 2018).

4-Experimental group (c) (Arachidonic acid group): (10) rats, were given AA only at a dose of 55µg/kg orally daily for a week, then once a week for the whole duration of the study (Gundala *et al.,* 2018).

Female rats were mated with one male overnight, and the presence of a vaginal plug that contains sperm was considered gestational day zero.

For each group, the female pregnant rats were sacrificed at the following ages: gestational days 15, 17 and 19. The animals were anaesthetized by ether inhalation, then intracardiac perfusion with normal saline was performed and the fetuses were collected for further investigation. All experimental procedures were approved by the Institutional Ethics Committee of the faculty of medicine at Assiut University (Approval No 17200437).

We measured the weight, snout-rump length, crown-heel, and crown-rump in order to perform statistical analysis. The statistical analysis was carried out using version 5 of GraphPad Prism software. The information was displayed as mean ± standard deviation (SD). To compare the groups, One-Way Analysis of Variance (ANOVA) was employed, and then the Bonferroni posthoc test was performed. P-values less than 0.05 indicated statistical significance.

Histological Study:

The sacrum and lumbar vertebrae were removed at each of the previous ages. For a period of 24 to 72 hours, they were preserved in 10% formalin solution for light microscopic study and 2.5% glutaraldehyde for electron microscopy.The bone samples were ready to be embedded in paraffin. Haematoxylin and Eosin-stained sections (8–10µ) were done to show the overall histological structure; Masson's trichrome stained sections were done to show the collagen fibers; and semithin sections (1 micron) stained with toluidine blue were performed to show the cartilage matrix's glycosaminoglycan content. All stained slides were examined with an Olympus CX41 microscope, and images of the slides under the microscope were taken with an Olympus DP72 CCD digital camera (Olympus Corporation, Tokyo, Japan) at the Human Anatomy and Embryology Department, Faculty of Medicine, Assiut University, Egypt.

For a transmission electron microscopy (TEM) analysis, ultra-thin slices (450–500 Å) of the epiphyseal growth plate of the sixth lumbar vertebrae of the 19-day-old fetus were produced to evaluate the chondrocytes. The stained ultrathin sections were viewed using the Jeol-JEM-100 CXII electron microscope (JEOL, Tokyo, Japan), and pictures were captured at the Electron Microscopy Unit of Assiut University in Egypt.

RESULTS

Morphological Results:

Morphometrical and statistical analysis of the weight and lengths of the crown heel, snout rump, and crown-rump of the 15-day-old (Table 1) (Figs. 1 & 2), 17-day-old (Table 2) (Figs. 3 & 4) and 19-day-old (Table 3) (Figs. 5 & 6) fetuses showed a highly significant decrease ($p < 0.0001$) in all parameters in the alloxan-induced diabetes groups as compared to the control groups. Whereas, both the alloxan + arachidonic acid group and the arachidonic acid-only group of the three age groups showed a nonsignificant difference when contrasted to the control group.

Haematoxylin and Eosin (H&E) Stain:

In the Haematoxylin and Eosin-stained sagittal sections of the lumbar (L5&L6) (Figs. 7 & 9) and the sacral (S1&S2) (Figs. 8 & 10) vertebrae of the control group, the alloxan + arachidonic acid group and the arachidonic acid only group of the 15 and the 17 days old

albino rat fetus, the vertebral body appeared wholly cartilaginous.

The chondrocytes in the epiphysis are arranged as follows:

1- The reserve cell zone: This zone contains tiny, spindle- or rounded-shaped cells that can be detected both inside and outside of the lacuna.

2- Proliferative cell zone: This zone is characterized by flattened cells that are encased in lacunae and arranged in a distinctive columnar pattern parallel to the growth axis.

3- Hypertrophied cell zone: Compared to earlier cells, the hypertrophied chondrocytes are bigger. They are surrounded by huge, spherical lacunae.

In the Haematoxylin and Eosin-stained sagittal sections of the lumbar (L5&L6) (Fig. 11) and the sacral (S1&S2) (Fig. 12) vertebrae of the control group, the alloxan + arachidonic acid group and the arachidonic acid only group of the 19-day-old albino rat fetus, the vertebral body appears with central centrum and two outer regions of hyaline cartilage (epiphysis). The chondrocytes in the epiphyses are arranged into four zones: the zone of reserve cells, the zone of proliferative cells, the zone of hypertrophied cells and the calcification zone (in this zone, degeneration of hypertrophied chondrocytes occurs leaving lacunae which are then attacked by cells from the marrow filled gaps of the centrum). Each vertebra's centrum (Figs. 11 & 12) displays a major center of ossification that is well-developed, with many gaps in the calcified cartilage that signify empty confluent lacunae following chondrocyte degeneration.

The Haematoxylin and Eosin-stained sagittal sections of the lumbar (L5&L6) (Fig. 7b) and the sacral (S1&S2) (Fig. 8b) vertebrae of the alloxan-induced diabetic group of the 15-day-old albino rat fetus show delayed development (delayed chondrification) with shrunken and mesenchymal bodies. The mesenchymal cells show vacuolated cytoplasm. Remnants of the notochord appear in the lumbar vertebrae.

The Haematoxylin and Eosin-stained sagittal sections of the lumbar (L5&L6) (Fig. 9b) and the sacral (S1&S2) (Fig. 10b) vertebrae of the alloxan-induced diabetic group of the 17-day-old albino rat fetus are shrunken as compared to the control group. Remnants of the notochord appeared in the sacral vertebrae. The developing chondrocytes were distorted. They appeared smaller with vacuolated cytoplasm. The regions of the matrix that were cell-free could be seen.

The Haematoxylin and Eosin-stained sagittal sections of the lumbar (L5&L6) (Fig. 11b) and the sacral (S1&S2) (Fig. 12b) vertebrae of the alloxan-induced diabetic group of the 19-day-old albino rat fetus showed completely cartilaginous vertebrae with delayed development of the primary ossification center. The vertebrae are shrunken as contrasted to the control group. Remnants of the notochord appear in the sacral vertebrae. The developing chondrocytes are distorted and appear smaller with vacuolated cytoplasm. Furthermore, portions of the matrix devoid of cells and empty lacunae are seen.

Masson's Trichrome Stain:

In Masson's trichrome-stained sagittal sections of the lumbar (L5&L6) (Figs. 13, 15 & 17) and the sacral (S1&S2) (Figs. 14, 16 & 18) vertebrae of the control group, the alloxan + arachidonic acid group and the arachidonic acid only group of the three studied age groups, the epiphyses show normal even spreading of green color stain in the matrix among the developing chondrocytes. The intervertebral disc (Figs. 13-18) appears to be comprised of a gelatinous core (nucleus pulposus) and an outer layer (annulus fibrosus).

Masson's trichrome-stained sagittal sections of the lumbar (L5&L6) (Fig. 13b) and the sacral (S1&S2) (Fig. 14b) vertebrae of the alloxan-induced diabetic group of the 15-day-old albino rat fetus illustrate absent staining of the matrix in between the mesenchymal cells. In addition, diminished staining of

the matrix among the developing chondrocytes is observed in Masson's trichrome-stained sagittal sections of the lumbar (L5&L6) (Figs. 15b & 17b) and the sacral (S1&S2) (Figs. 16b & 18b) vertebrae of the alloxan-induced diabetic group of the 17- and the 19-day-old albino rat fetus.

Delayed development of the intervertebral disc (Fig. 14b) is observed in the sacral vertebrae of the alloxan-induced diabetic group of the 15-day-old albino rat fetus.

Toluidine Blue Stain:

Semithin sections of the 6th lumbar vertebral epiphysis (Fig. 19) of the control group, the alloxan + arachidonic acid group and the arachidonic acid only group of the 19-day-old albino rat fetus illustrate normal spreading of the Toluidine blue stain in the matrix of the cartilage. Decreased staining of the cartilage matrix is seen in the semithin sections of the 6th lumbar vertebral epiphysis (Fig. 19b) of the alloxan-induced diabetic group of the 19-day-old albino rat fetus when compared to the control group.

Electron Microscopic Examination:

Electron microscopic examination of the epiphyseal reserve cell zone of the 6th lumbar (Figs. 20 & 21) of the control group, the alloxan + arachidonic acid group and the arachidonic acid only group of the 19-day-old albino rat fetus reveals well-formed nucleus, rough endoplasmic reticulum and lipid granules evident in the cytoplasm with numerous cytoplasmic processes. There was a small, transparent pericellular area all around the cells. The extracellular matrix had a delicate network of thin fibrils outside of this area.

The reserve cell of the alloxan-induced diabetic group (Figs. 20b & 21b) of the 19-day-old albino rat fetus showed shrinkage of the cell with an abnormal outline, cytoplasmic vacuolations, shrunken nucleus and less developed rough endoplasmic reticulum. The surrounding pericellular space appears widened.

Table 1: compares the weight, crown heel length, snout rump length, and crown-rump length of the 15-day-old rat fetus in the control group and groups that received arachidonic acid alone, alloxan+arachidonic acid, and alloxan.

Group	Control	Alloxan-induced diabetes	Alloxan+Arachidonic Acid	Arachidonic Acid only	ANOVA
	mean± SD	mean± SD	mean± SD	mean± SD	P value
Weight (gm)	1.54±0.15	0.78±0.11	1.53±0.19	1.56±0.15	<0.0001
Crown-rump length (cm)	2.37±0.05	1.30±0.06	2.33±0.05	2.40±0.06	<0.0001
Snout rump length (cm)	1.78±0.12	0.73±0.08	1.75±0.08	1.82±0.10	<0.0001
Crown heel length (cm)	2.65±0.05	1.58±0.08	2.62±0.08	2.68±0.08	<0.0001

(SD) standard deviation

***P≤0.0001 highly significant

**P≤ 0.001 moderately significant

Table 2: compares the weight, crown heel length, snout rump length, and crown-rump length of the 17-day-old rat fetus in the control, alloxan-induced diabetes, alloxan+arachidonic acid and arachidonic acid only groups.

Group	Control	Alloxan-induced diabetes	Alloxan+Arachidonic Acid	Arachidonic Acid only	ANOVA
	mean± SD	mean± SD	mean± SD	mean± SD	P value
Weight (gm)	2.36±0.08	1.11±0.06	2.36±0.07	2.37±0.08	<0.0001
Crown-rump length (cm)	3.10±0.28	2.02±0.31	3.02±0.32	3.17±0.31	<0.0001
Snout rump length (cm)	2.70±0.28	1.67±0.26	2.63±0.30	2.77±0.27	<0.0001
Crown heel length (cm)	3.53±0.08	2.68±0.39	3.47±0.12	3.60±0.06	<0.0001

(SD) standard deviation
***P≤0.0001 highly significant
**P≤ 0.001 moderately significant.

Table 3: compares the weight, crown heel length, snout rump length, and crown-rump length of the 19-day-old rat fetus in the control, alloxan-induced diabetes, alloxan+arachidonic acid and arachidonic acid only groups.

Group	Control	Alloxan-induced diabetes	Alloxan+Arachidonic Acid	Arachidonic Acid only	ANOVA
	mean± SD	mean± SD	mean± SD	mean± SD	P value
Weight (gm)	4.15±0.46	2.32±0.53	4.13±0.47	4.35±0.45	<0.0001
Crown-rump length (cm)	3.65±0.12	2.63±0.14	3.58±0.08	3.68±0.16	<0.0001
Snout rump length (cm)	3.25±0.14	2.23±0.14	3.20±0.11	3.30±0.15	<0.0001
Crown heel length (cm)	4.25±0.14	3.20±0.11	4.22±0.17	4.30±0.17	<0.0001

(SD) standard deviation
***P≤0.0001 highly significant
**P≤ 0.001 moderately significant

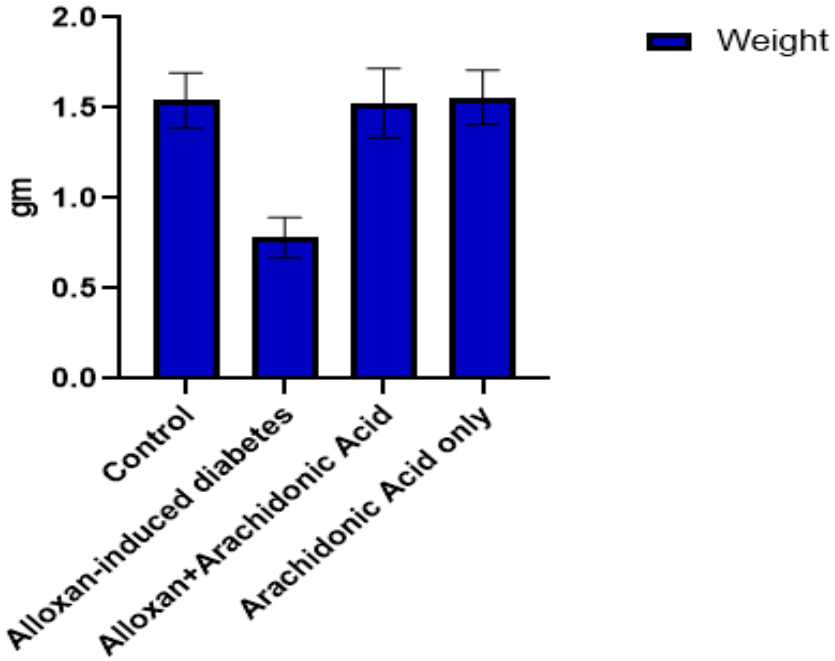

Fig.1: compares the weights of the 15-day-old rat fetuses in the control, alloxan-induced diabetes, alloxan+arachidonic acid, and arachidonic acid-only groups.

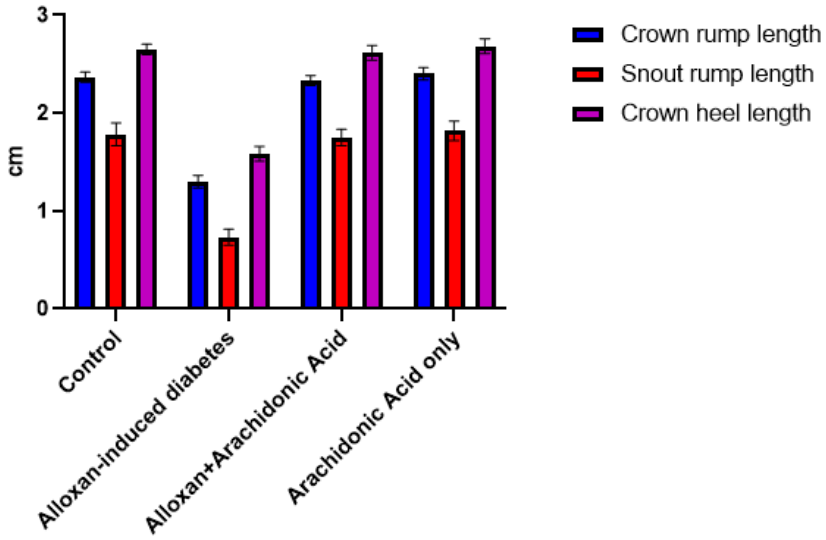

Fig.2: compares the lengths of the crown heel, snout rump, and crown-rump of the 15-day-old rat fetus in the groups that received arachidonic acid alone, alloxan+arachidonic acid, alloxan and control (alloxan-induced diabetes).

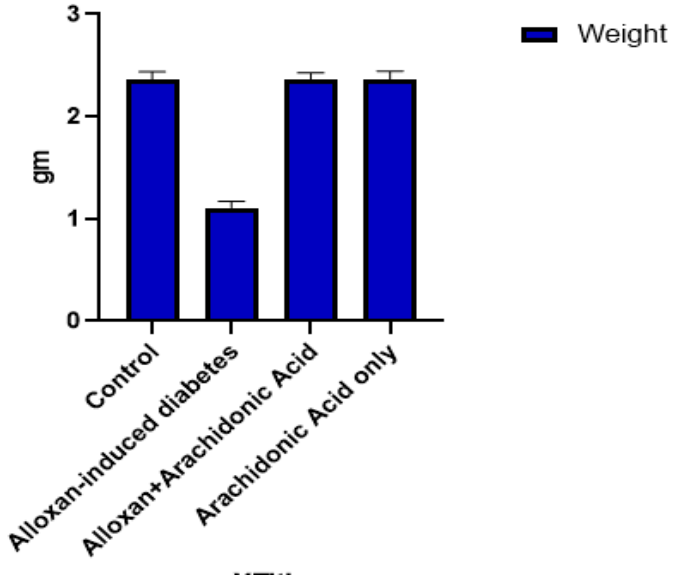

Fig.3: compare the weights of the 17-day-old rat fetuses in the control, alloxan-induced diabetes, alloxan+arachidonic acid, and arachidonic acid-only groups.

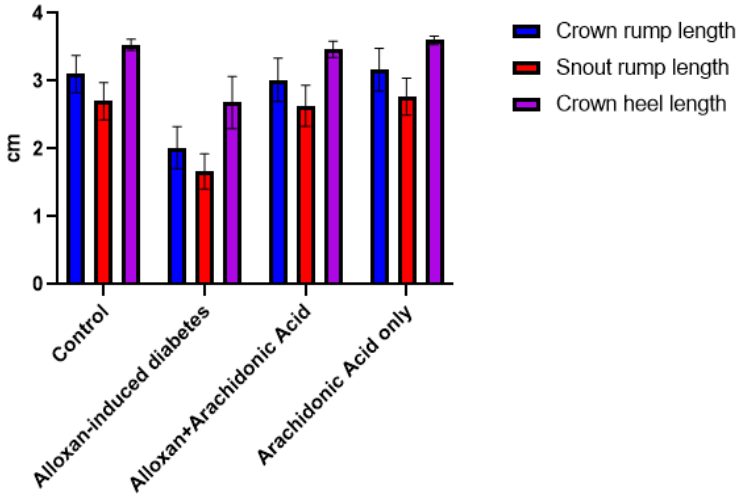

Fig. 4: compares the lengths of the crown rump, snout rump, and crown heel of the 17-day-old rat fetuses in the control, alloxan-induced diabetes, alloxan+arachidonic acid, and arachidonic acid-only groups.

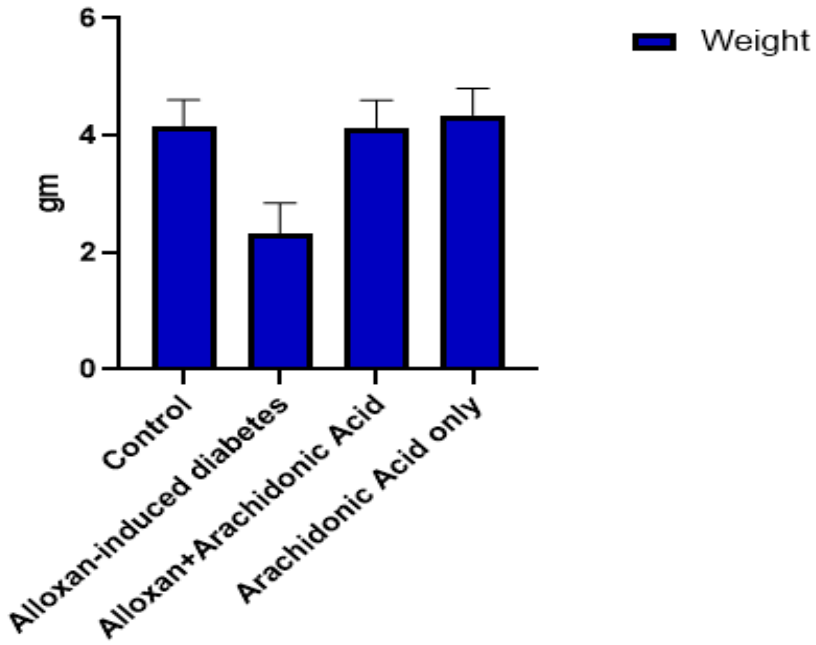

Fig. 5: compares the weight of the 19-day-old rat fetus in the groups that received arachidonic acid only, alloxan+arachidonic acid, alloxan, and control.

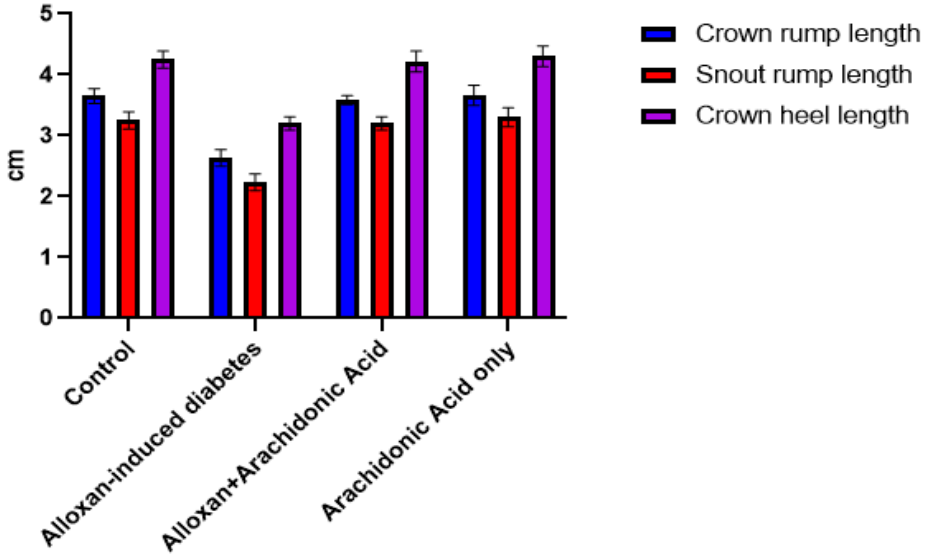

Fig. 6: compares the crown heel length, snout rump length, and crown-rump length of the 19-day-old rat fetus in the arachidonic acid only, alloxan+arachidonic acid, alloxan-induced diabetes and control groups.

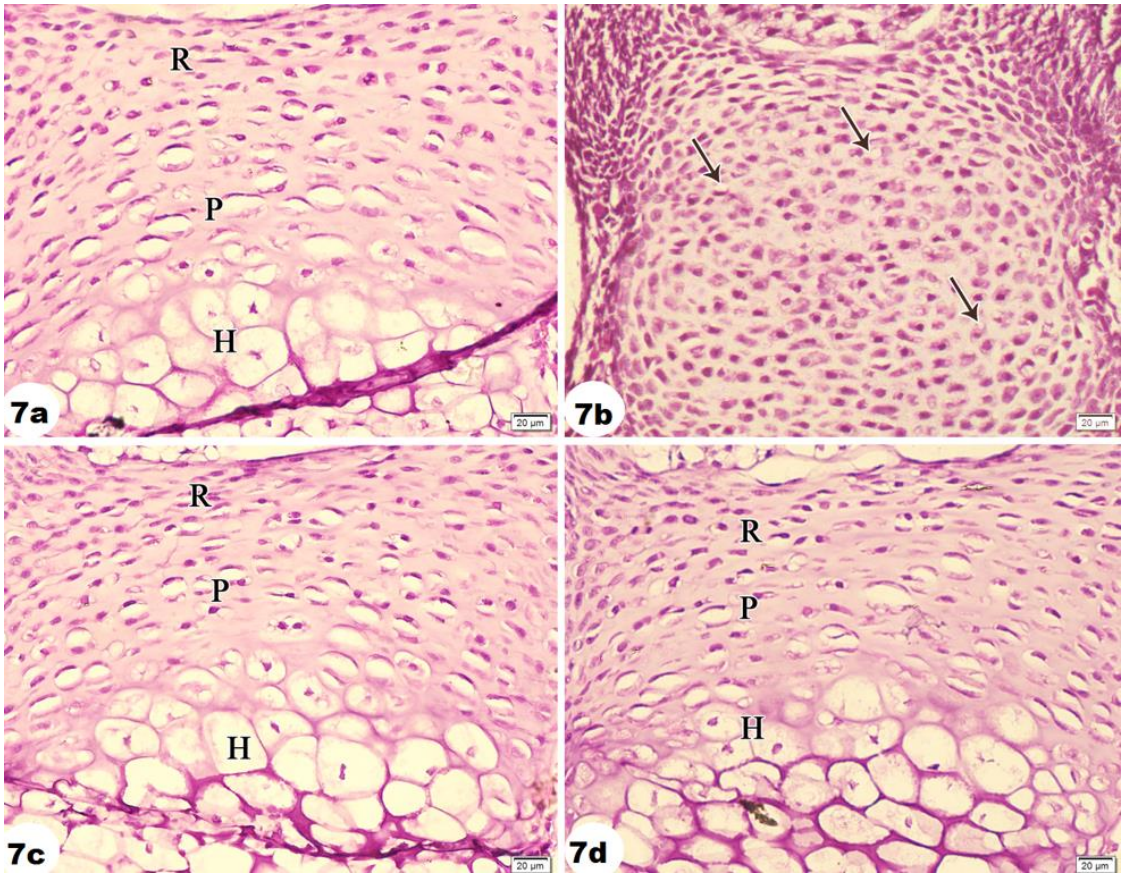

Fig. (7): A photomicrograph of the sagittal section of the sixth lumbar vertebra of a 15-day-old albino rat fetus in the control group **(7a)**, the alloxan-induced diabetic group **(7b)**, the alloxan + arachidonic acid group **(7c)** and the arachidonic acid only group **(7d)** show normal growing chondrocytes: reserve cells (R), proliferative cells (P), and hypertrophied cells (H). Mesenchymal cells with vacuolated cytoplasm (arrow) are seen in the alloxan-induced diabetes group (b). (H&E, X400)

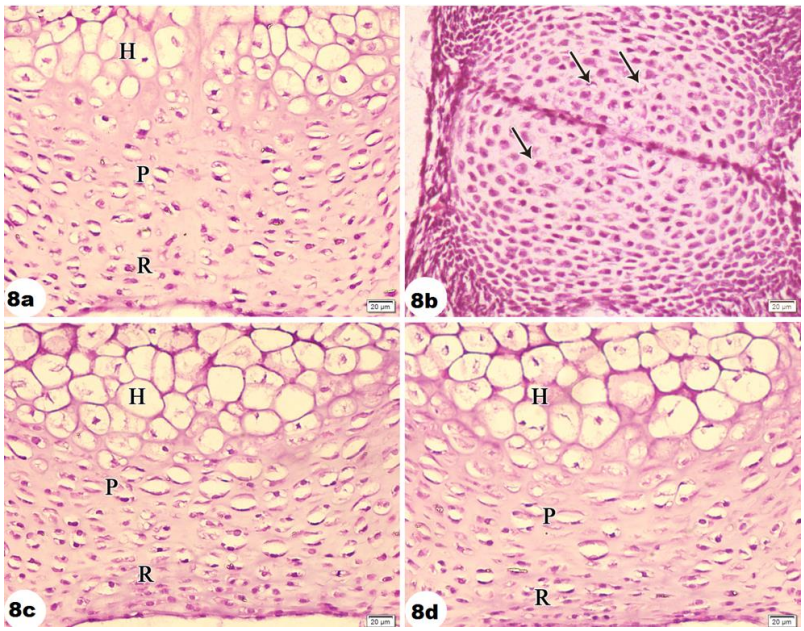

Fig. (8) shows a photomicrograph of the sagittal section of the first sacral vertebra of a 15-day-old albino rat fetus in the control group **(8a)**, the alloxan-induced diabetic group **(8b)**, the alloxan + arachidonic acid group **(8c)** and the arachidonic acid only group **(8d)**. The epiphyses of the control group **(8a)**, alloxan + arachidonic acid group **(8c)**, and arachidonic acid only group **(8d)** display proliferative cells (P), reserve cells (R), and hypertrophied cells (H). Conversely, mesenchymal cells exhibiting vacuolated cytoplasm (arrow) are noted in the group with alloxan-induced diabetes **(8b)**. (H&E, X400).

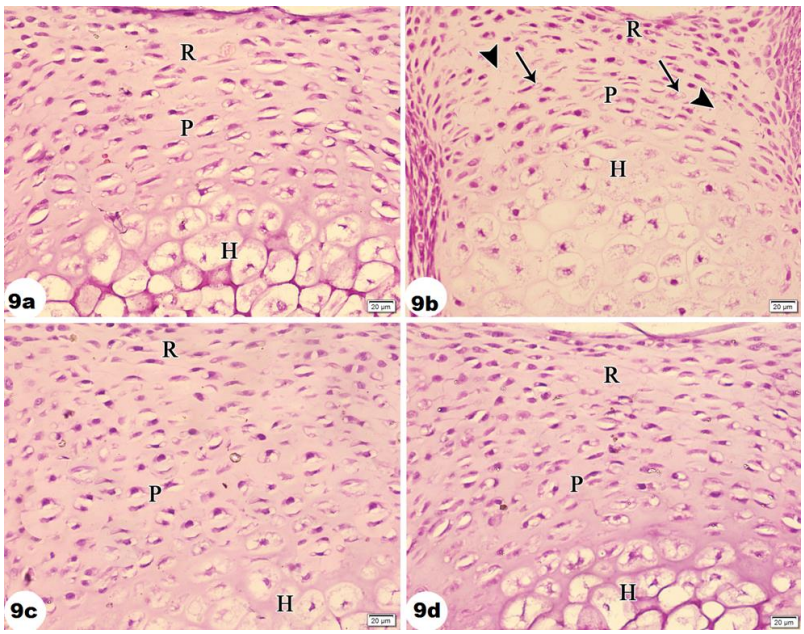

Fig. (9): A photomicrograph of a sagittal section of the epiphyseal growth plate of the sixth lumbar vertebra of a 17-day-old albino rat fetus of the control group **(9a)**, the alloxan-induced diabetic group **(9b)**, the alloxan + arachidonic acid group **(9c)** and the arachidonic acid only group **(9d)**. It demonstrates the growth of chondrocytes. Reserve cells (R), proliferative cells (P) and hypertrophied cells (H). The epiphyses of the alloxan-induced diabetic group **(9b)** show distortion and disorganization of the growing chondrocytes, which appear smaller with vacuolated cytoplasm (arrow). In contrast, the epiphyses of the control group **(9a)**, the alloxan + arachidonic acid group **(9c)**, and the arachidonic acid-only group **(9d)** show normal cells. Note: In the alloxan-induced diabetic group (b), there are patches of the matrix devoid of cells (arrowhead). (H&E, X400)

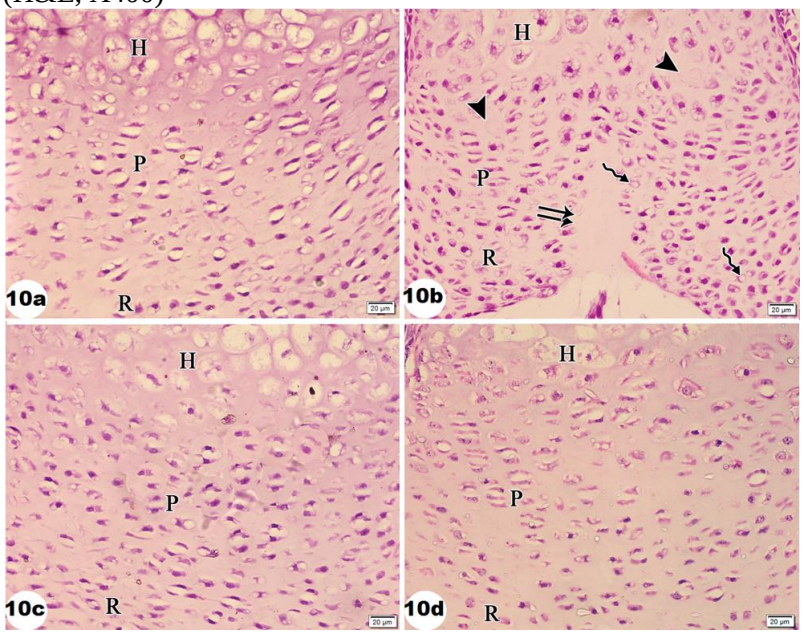

Fig.10: shows a photomicrograph of a sagittal section of the epiphysis of the first sacral vertebra of a 17-day-old albino rat fetus in the control group **(10a)**, diabetic group **(10b)**, alloxan + arachidonic acid group **(10c)**, and arachidonic acid only group **(10d)**. It shows growing chondrocytes: reserve cells (R), proliferative cells (P), and hypertrophied cells (H). In the epiphyses of the control group **(10a)**, alloxan + arachidonic acid group **(10c)**, and arachidonic acid only group **(10d)**, normal cells are visible. On the other hand, the diabetic group **(10b)** caused by alloxan exhibits distortion and disarray of the developing chondrocytes, which look smaller with the presence of notochord remains (double arrow). Regions of the matrix without cells (arrowhead) and empty lacunae (wavy arrow) were observed in the alloxan-induced diabetic group. (H&E, X400)

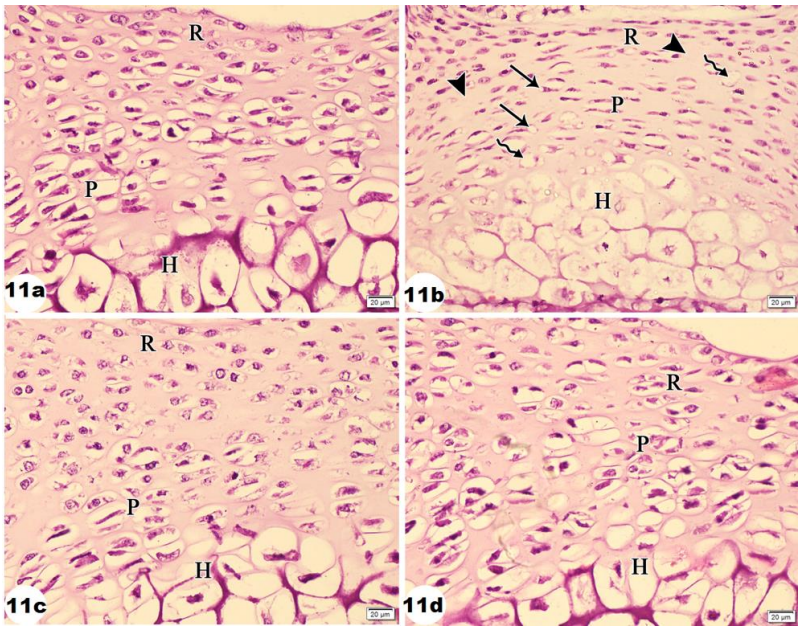

Fig.11: A photomicrograph showing the growth of chondrocytes, reserve cells (R), proliferative cells (P), and hypertrophied cells (H), in a sagittal section of the epiphysis of the 6th lumbar vertebra of a 19-day-old albino rat fetus in the control group **(11a)**, alloxan-induced diabetic group **(11b)**, alloxan + arachidonic acid group **(11c)**, and arachidonic acid group **(11d)**. The epiphyses of the alloxan-induced diabetic group **(11b)** show distortion and disorganization of the growing chondrocytes, which appear smaller with vacuolated cytoplasm (arrow). In contrast, the epiphyses of the control group **(11a)**, the alloxan + arachidonic acid group **(11c)**, and the arachidonic acid-only group **(11d)** show normal cells. Note: in the alloxan-induced diabetic group **(11b)**, empty lacunae (wavy arrow) and portions of the matrix without any cells (arrowhead). (H&E, X400)

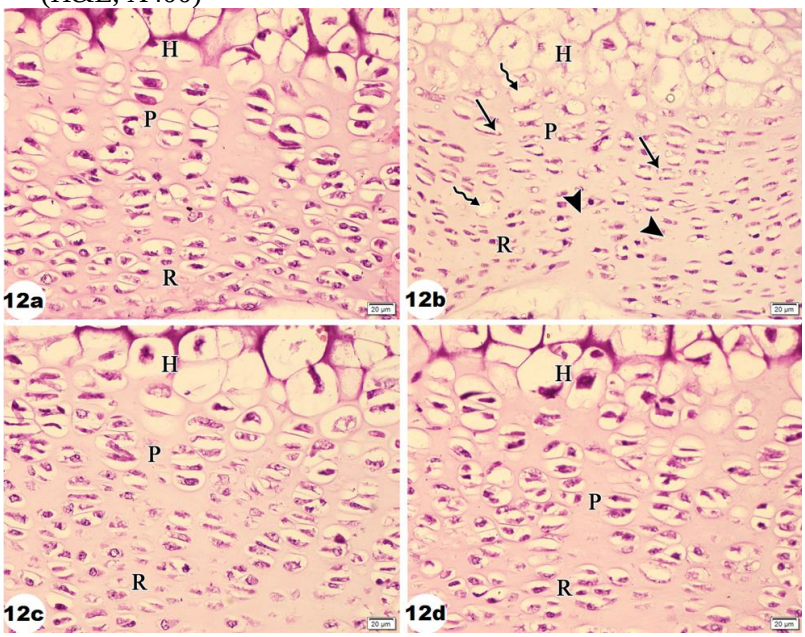

Fig. (12): A photomicrograph of a sagittal section of the epiphysis of the first sacral vertebra of a 19-day-old albino rat fetus showing growing chondrocytes: reserve cells (R), proliferative cells (P), and hypertrophied cells (H). The control group **(12a)**, alloxan-induced diabetic group **(12b)**, alloxan + arachidonic acid group **(12c)**, and arachidonic acid only group **(12d)**. Normal cells can be seen in the epiphyses of the arachidonic acid-only group **(12d)**, the alloxan + arachidonic acid group **(12c)**, and the control group **(12a)**. The alloxan-induced diabetes group **(12b)** exhibits small, deformed, and disordered developing chondrocytes with vacuolated cytoplasm (arrow). The diabetic group **(12b)** exhibits empty lacunae (wavy arrow) and portions of the matrix devoid of cells (arrowhead). (H&E, X400)

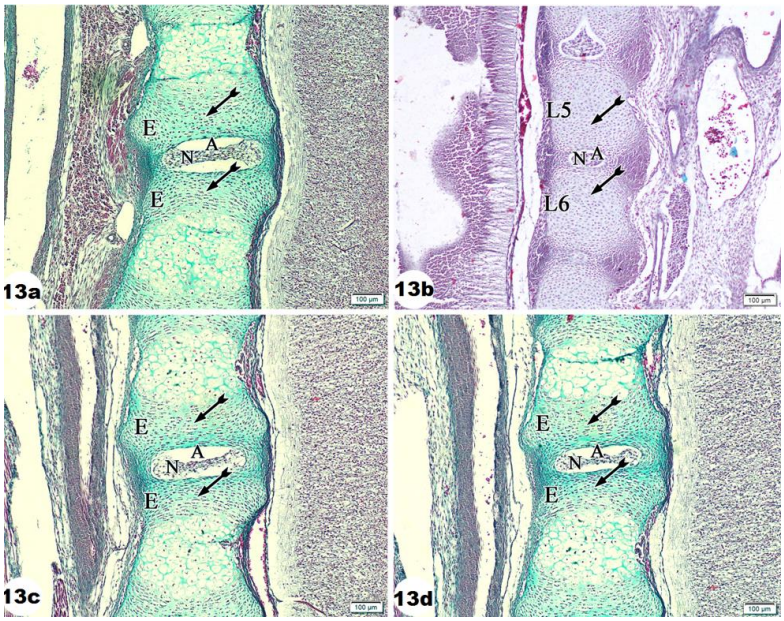

Fig. (13): A photomicrograph of the sagittal section of the fifth and sixth lumbar vertebrae of a 15-day-old albino rat fetus in the control group **(13a)**, alloxan-induced diabetic group **(13b)**, alloxan + arachidonic acid group **(13c)**, and arachidonic acid only group **(13d)**. The control group's **(13a)**, alloxan + arachidonic acid group's **(13c)**, and arachidonic acid only group's **(13d)** vertebrae all exhibit a normal, homogeneous stain distribution with green matrix color (tailed arrow) between the developing chondrocytes in their epiphyses (E). On the other hand, the mesenchymal cells of the vertebrae of the alloxan-induced diabetes group **(13b)** do not exhibit any staining of the matrix (tailed arrow). NB: the nucleus pulposus (N) and annulus fibrosus (A) of the intervertebral disc. (Masson's trichrome, X100)

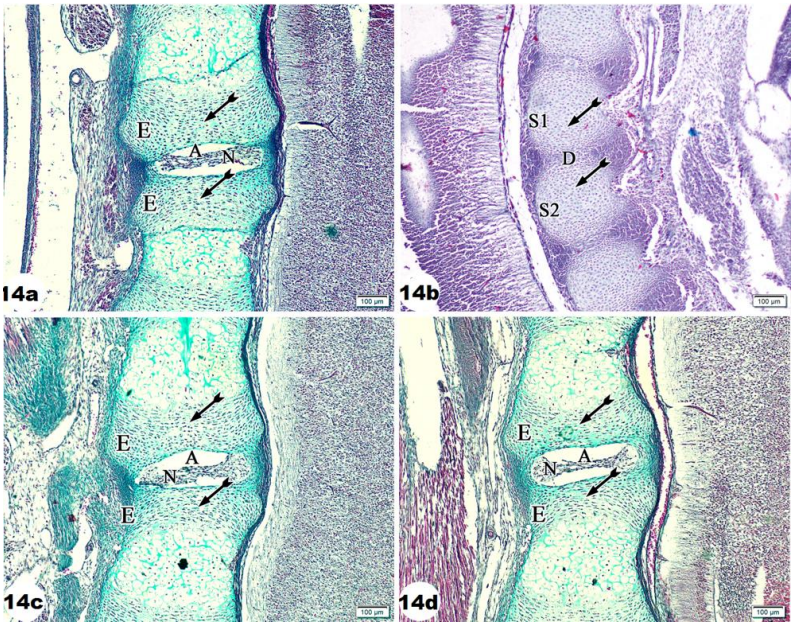

Fig. (14): A photomicrograph of the sagittal section of the first and second sacral vertebrae of a 15-day-old albino rat fetus in the control group **(14a)**, the alloxan-induced diabetic group **(14b)**, the alloxan + arachidonic acid group **(14c)** and the arachidonic acid only group **(14d)**. The vertebrae of the control group **(14a)**, alloxan + arachidonic acid group **(14c)**, and arachidonic acid only group **(14d)** all exhibit a normal, homogeneous distribution of the green stain in the cartilage matrix (tailed arrow) of the epiphyses (E). The nucleus pulposus (N) and annulus fibrosus (A) combine to produce the intervertebral disc. But the alloxan-induced diabetic group's vertebrae **(14b)** lack the matrix's staining (tailed arrow) between the mesenchymal cells (S1 & S2), with delayed development of the intervertebral disc (D). (Masson's trichrome, X100)

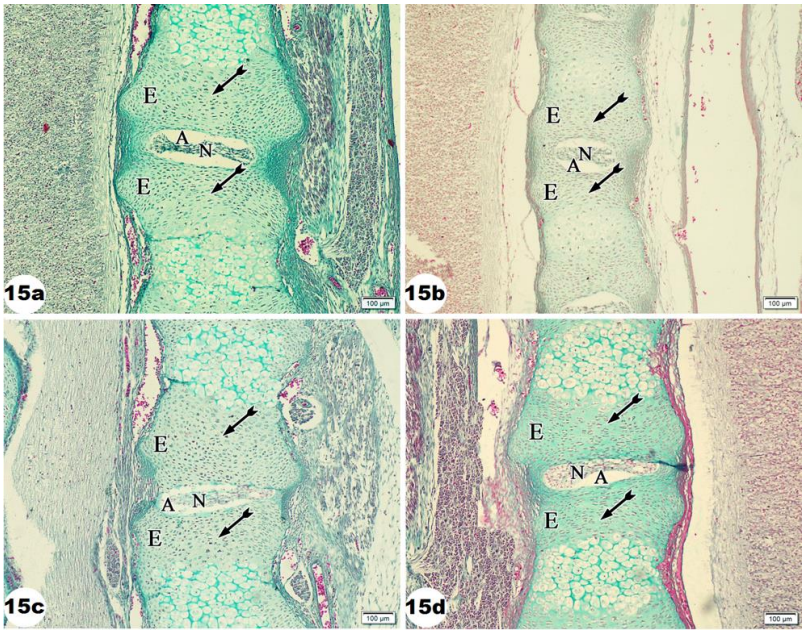

Fig. (15): A photomicrograph depicting the sagittal section of the fifth and sixth lumbar vertebrae of an albino rat fetus, aged 17 days, in four groups: the control group **(15a)**, the alloxan-induced diabetes group **(15b)**, the alloxan + arachidonic acid group **(15c)**, and the arachidonic acid only group **(15d)**. The usual homogeneous distribution of the green color in the matrix (tailed arrow) between the growing chondrocytes is depicted by the epiphyses (E) of the vertebrae of the control group **(15a)**, the alloxan + arachidonic acid group **(15c)**, and the arachidonic acid only group **(15d)**. The vertebrae of the alloxan-induced diabetes group **(15b)** show diminished cartilage matrix staining (tailed arrow). NB: the intervertebral disc's nucleus pulposus (N) and annulus fibrosus (A). (Masson's trichrome, X100) .

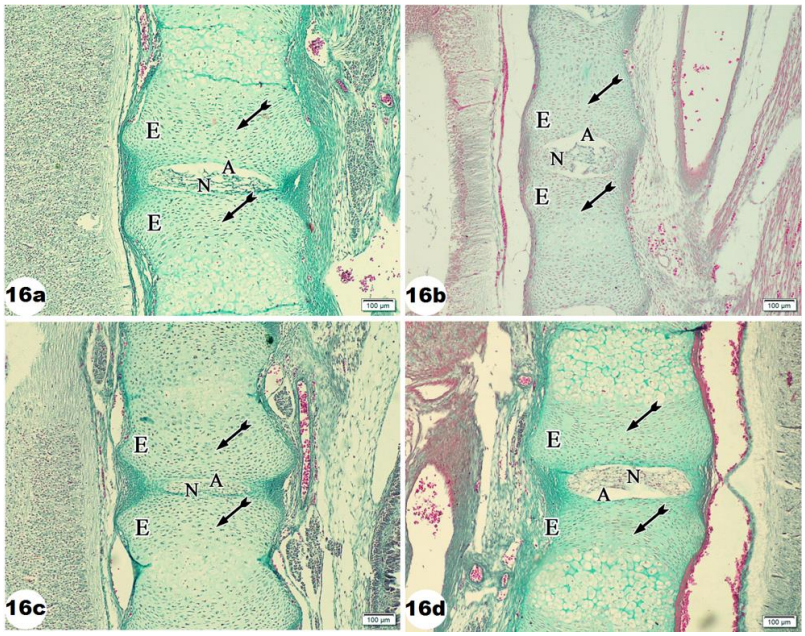

Fig. (16) shows a photomicrograph demonstrating the epiphyses (E1 & E2) of the first and second sacral vertebrae of a 17-day-old albino rat fetus in the control group **(16a)**, alloxan-induced diabetes group **(16b)**, alloxan + arachidonic acid group **(16c)**, and arachidonic acid only group **(16d)**. In the matrix of the epiphysis, the vertebrae of the control group **(16a)**, the alloxan + arachidonic acid group **(16c)**, and the arachidonic acid only group **(16d)** exhibit a normal, uniform stain distribution (tailed arrow). On the other hand, the developing chondrocytes among the vertebrae of the alloxan-induced diabetes group **(16b)** exhibit less staining of the matrix (tailed arrow). NB: the nucleus pulposus (N) and annulus fibrosus (A) of the intervertebral disc. (Masson's trichrome, X100)

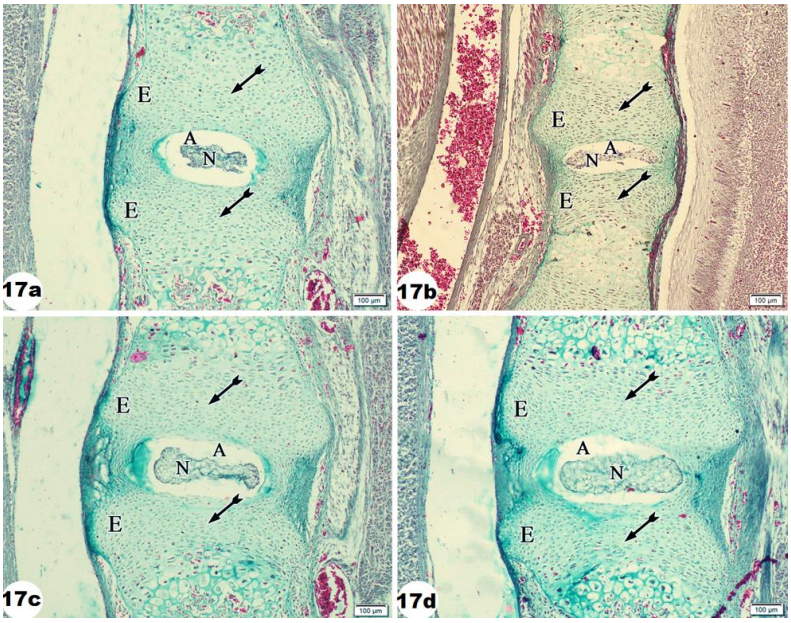

Fig. (17) shows a photomicrograph of the sagittal section of the fifth and sixth lumbar vertebrae of a 19-day-old albino rat fetus in the control group **(17a)**, the alloxan-induced diabetic group **(17b)**, the alloxan + arachidonic acid group **(17c)** and the arachidonic acid only group **(17d)**. The epiphyses (E) of the control group **(17a)**, the alloxan + arachidonic acid group **(17c)**, and the arachidonic acid only group **(17d)** show a normal, homogeneous distribution of the stain with the green color of the matrix (tailed arrow) in between the developing chondrocytes. In the epiphysis of the alloxan-induced diabetes group **(17b)**, there is diminished Masson staining (tailed arrow). NB: the intervertebral disc's nucleus pulposus (N) and annulus fibrosus (A). (Masson's trichrome, X100)

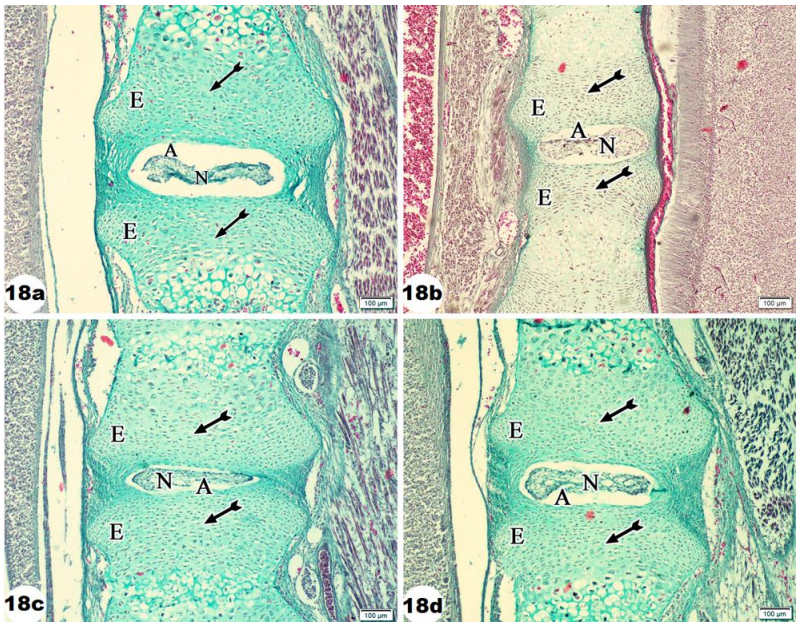

Fig. (18) shows a photomicrograph of a sagittal section displaying the epiphyses (E) of the first and second sacral vertebrae of a 19-day-old albino rat fetus in the control group **(18a)**, diabetes group **(18b)**, alloxan + arachidonic acid group **(18c)**, and arachidonic acid exclusive group **(18d)**. The green color in the matrix (tailed arrow) between the proliferating chondrocytes is distributed normally and homogeneously in the control group **(18a)**, alloxan + arachidonic acid group **(18c)**, and arachidonic acid only group **(18d)**. On the other hand, the epiphysis of the alloxan-induced diabetes group **(18b)** shows reduced staining of the cartilage matrix (tailed arrow). NB: the nucleus pulposus (N) and annulus fibrosus (A) of the intervertebral disc. (Masson's trichrome, X100)

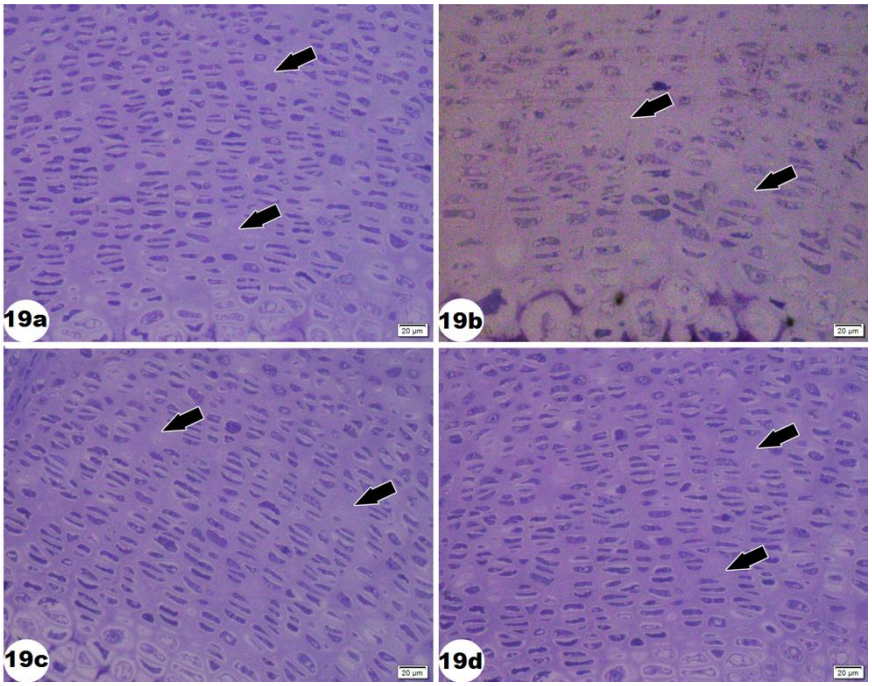

Fig. 19: shows semithin sections of the epiphysis of the sixth lumbar vertebra of a 19-day-old albino rat belonging to the control group **(19a)**, the alloxan-induced diabetic group **(19b)**, the alloxan + arachidonic acid group **(19c)**, and the arachidonic acid only group **(19d)**. The thick arrows in the control group **(19a)**, the alloxan + arachidonic acid group **(19c)**, and the arachidonic acid-only group **(19d)** show a normal distribution of the Toluidine blue stain in the cartilage matrix. On the other hand, the epiphysis of the alloxan-induced diabetes group **(19b)** has less cartilage matrix staining (thick arrow). (Toluidine blue,X400)

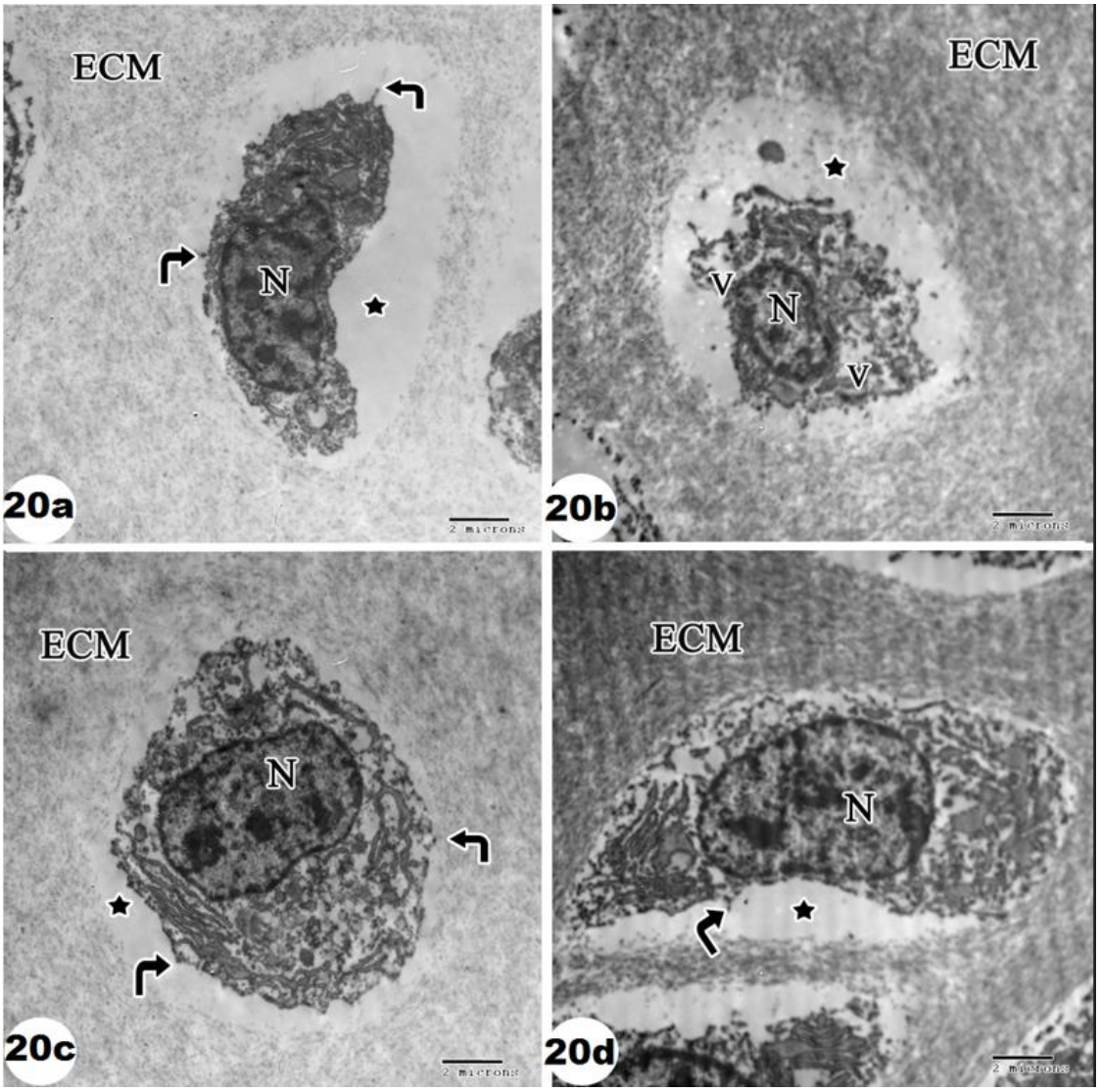

Fig. (20) shows an electron micrograph of the reserve cell zone of the epiphysis of the sixth lumbar vertebra of a 19 days old albino rat fetus of the control group **(20a)**, the alloxan-induced diabetic group **(20b)**, the alloxan + arachidonic acid group **(20c)** and the arachidonic acid only group **(20d)**. The reserve cells of the control group **(20a)**, the alloxan + arachidonic acid group **(20c)** and the arachidonic acid only group **(20d)** show multiple cytoplasmic processes **(curved arrows)**, well-formed nucleus (N)**,** pericellular space **(asterisk)** and extracellular matrix **(ECM)** rich in collagen fibrils**.** The reserve cell of the alloxan-induced diabetic group **(20b)** shows a shrunken reserve cell with a shrunken nucleus **(N),** cytoplasmic vacuolations (V) and widened pericellular space **(asterisk).** (TEM, X4800)

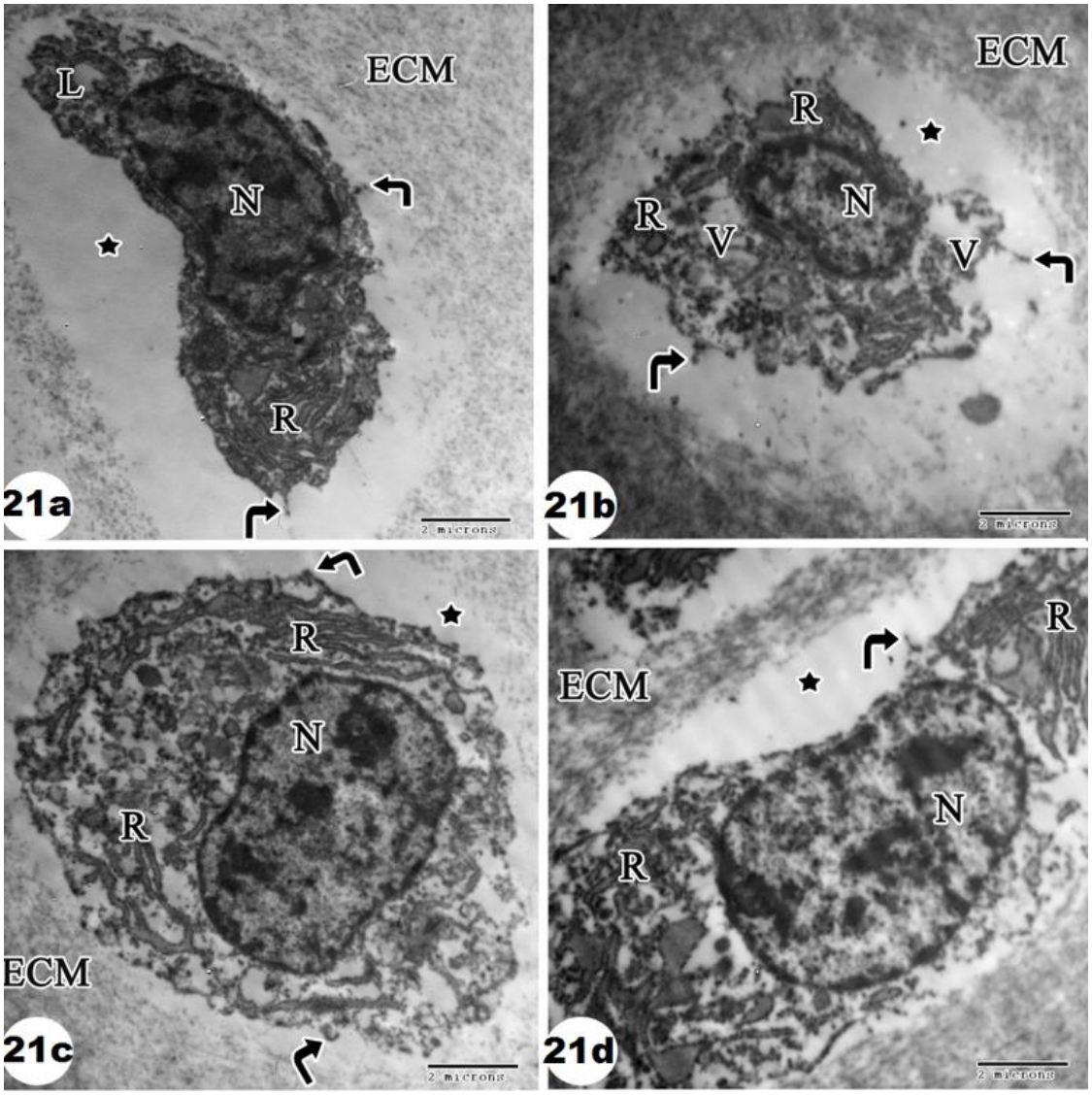

Fig. (21) shows an electron micrograph of the reserve cell zone of the epiphysis of the sixth lumbar vertebra of a 19-day-old albino rat fetus in the control group **(21a)**, the alloxan-induced diabetic group **(21b)**, the alloxan + arachidonic acid group **(21c)** and the arachidonic acid only group **(21d)**. The reserve cells in the control group **(21a)**, alloxan + arachidonic acid group **(21c)**, and arachidonic acid only group **(21d)** have many cytoplasmic processes (curved arrows) and a well-formed nucleus (N), rough endoplasmic reticulum (R), and lipid granules (L) visible in the cytoplasm. Furthermore, extracellular matrix (ECM) rich in collagen fibrils and pericellular space (asterisk) are observed. The diabetic group **(21b)** caused by alloxan exhibits a shrunken reserve cell with an uneven contour, a shrunken nucleus (N), cytoplasmic vacuolations (V), less developed rough endoplasmic reticulum **(R),** widened pericellular space (asterisk). (TEM, X7200)

DISCUSSION

Diabetes in pregnancy is one of the important healthcare issues. The incidence of birth abnormalities increases two to five times in women with gestational diabetes, even with optimal diabetic care provided before and during pregnancy (Vinceti *et al.*, 2014). Pregnant women who already have diabetes are more likely to have infants with spine deformities (Aberg *et al.,* 2001), delayed fetal skeletal growth and retarded ossification (Sirasanagandla *et al.*, 2014).

In this work, morphometrical and statistical analysis of the weight, lengths of the crown heel, snout rump, and crown-rump of three prenatal ages (15, 17 and 19 days) illustrates a highly significant decrease in all parameters in the alloxan-induced diabetes group as contrasted to the other groups. These findings support those of Bamfo and Odibo (2011) who hypothesized that

maternal diabetes is complicated by fetal growth retardation.

In the control group of the present study, the Haematoxylin and Eosin-stained sagittal sections of the lumbar (L5&L6) and the sacral (S1&S2) vertebrae of the 15- and 17-day-old albino rat fetuses demonstrate wholly cartilaginous vertebral bodies with layers of growing chondrocytes (reserve cells, proliferative cells and hypertrophied cells).

According to Tani *et al.* (2020), while maturation happens during postnatal life, skeletal building and differentiation occur during embryonic and fetal phases. Mesenchymal cells are transformed into cartilage cells, which subsequently ossify, during the process of cartilaginous ossification, which forms the vertebrae. By day fourteen of pregnancy, all cartilaginous primordia of the vertebrae and ribs are generated, with the exception of the atlas body and the arches of the caudal vertebrae, which develop one day later.

In the control group of this study, the Haematoxylin and Eosin-stained sagittal sections of the lumbar (L5&L6) and the sacral (S1&S2) vertebrae of the 19-day-old albino rat fetus show the vertebral body with central part (ossification centrum) and two eccentrics of cartilage (epiphysis). These findings support those of Jones *et al.* (1991) and DeSesso and Scialli (2018) who demonstrated that ossification in the vertebral bodies occurs through bilateral ossification centers which start at the age of 16 days prenatal in the midthoracic region and proceed from there in caudal and cephalic directions.

The chondrocytes in the epiphysis of the control group in this study are organized into four zones: the calcification zone, hypertrophied cells, proliferative cells, and reserve cells. Small, spindle- or rounded-shaped reserve cells can be detected both inside and outside of the lacuna. With a distinctive columnar structure along the growth axis, the proliferating cells are flattened and encased by lacunae. Compared to the earlier cells, the hypertrophied cells are larger. They are surrounded by huge, spherical lacunae. The hypertrophied chondrocytes in the calcification zone degenerate, leaving lacunae that are invaded by cells from the marrow-filled centrum gaps. These results support the previous findings of Guevara-Morales *et al.* (2020) who clarified that the epiphyseal growth plate is made up of chondrocytes at various stages of development. Round in shape, resting zone chondrocytes serve as the stem-like cells that restock the proliferative chondrocyte pool. After assuming a flattened form, proliferative zone chondrocytes eventually finish dividing and finally differentiate into hypertrophic chondrocytes. Just before the blood vessels invade the chondrocyte lacuna, the hypertrophic chondrocytes calcify the extracellular matrix around them and go through apoptosis.

In the control group of this work, the intervertebral disc is made of an external fibrous layer and a gelatinous core. These results are concomitant with Treuting et al. (2018) who revealed that the intervertebral discs consist of an inner gelatinous core called the nucleus pulposus and an outside ring of fibrocartilage called the annulus fibrosus. The annulus fibrosus attaches to cartilage end plates on the adjacent bodies of the vertebrae.

In the present work, the Haematoxylin and Eosin-stained sagittal sections of the lumbar (L5&L6) and the sacral (S1&S2) vertebrae of the 15, 17 and 19-day fetuses of the alloxan-induced diabetic group show delayed development with shrunken bodies. The cells demonstrate distortion, disorganization and vacuolated cytoplasm with some regions of cell-free matrix. Remnants of notochord are also observed. The vertebrae of the 15-day-old rat fetus of the same group appear mesenchymal with delayed development of the intervertebral disc in the sacral vertebrae. The vertebrae of the 19-day-old rat fetus show delayed development of the primary ossification center. These

findings confirm those of Tsur *et al.* (2013) who illustrated that maternal diabetes is associated with fetal growth retardation with decreased bone ossification in the offspring originating from a decrease in the calcium content of embryonic bone tissues as diabetes and disturbance of vitamin D synthesis are closely associated. The disturbance of vitamin D synthesis is caused by a drop in serum 25-hydroxycholecalciferol concentrations which affect the differentiation of bone cells.

In the control group of this study, Masson's trichrome-stained sagittal sections of the lumbar and sacral vertebrae of the three prenatal age groups show intense green color in the matrix due to abundance of collagen fibers between the growing chondrocytes of epiphyseal plate, and was stained deep blue by Toluidine blue stain due to the matrix sulfur in proteoglycans and glycosaminoglycans as reported by Obeid *et al.* (2020).

The present study revealed the absence of matrix staining between the mesenchymal cells in the 15-day-old rat fetus and reduced matrix staining between the growing chondrocytes of the epiphyses of the prenatal ages (17 and 19 days) in Masson's trichrome stained sagittal sections of the lumbar and sacral vertebrae of the alloxan-induced diabetic group. Additionally, the alloxan-induced diabetes group of the 19-day-old rat fetus had less cartilage matrix staining in the semithin sections of the epiphyseal plate of the 6th lumbar vertebra than the control group. These results support the previous studies of Shanbhogue *et al.* (2015) who have shown that hyperglycemia can cause bone loss, a drop in bone density, and damage to the microarchitecture of the bones in rats. Kume *et al.* (2005) claimed that hyperglycemia also alters the collagen integrity and mineral makeup of bone, which results in an increase in fat and adipogenic mesenchymal stem cells in the marrow cavity.

The reserve cell zone of the epiphyseal plate of the 6th lumbar vertebra of the 19-day-old rat fetus, as examined under an electron microscope in the control group for this study, exhibits normal cells with a well-formed nucleus, a rough endoplasmic reticulum, and lipid granules that are visible in the cytoplasm with multiple cytoplasmic processes. There is a thin, transparent pericellular zone encircling each cell. The extracellular matrix has a delicate network of thin fibrils outside of this zone. These results are consistent with that of Hassanin (2018).

In this study, electron microscopic examination of the reserve cell of the 19-day-old rat fetus of the alloxan-induced diabetic group showed shrunken irregular cells, irregular nucleus, many cytoplasmic vacuolations and underdeveloped rough endoplasmic reticulum. The surrounding pericellular space appears widened. Similar findings were observed by El-Sayyad *et al.* (2015) who found that the chondrocytes in the hindlimb bones of the diabetic mothers' embryos were deformed, with vacuolated cytoplasm, severe cytoplasmic compartment disruption, and clumping of their nuclear chromatin, which indicated apoptosis.

King (2012) revealed that Alloxan's diabetic effect is mostly linked to its quick uptake by beta cells, which increases the creation of free radicals and reactive oxygen species. These molecules cause beta cell DNA fragmentation and apoptosis, which leads to type 1 diabetes, which is characterized by hyperglycemia and low endogenous insulin secretion.

Several cellular abnormalities in the embryo are connected to the teratogenic process of diabetic pregnancy. Diabetes raises oxidative stress (Yang *et al.*, 1997), increases lipid peroxidation (Cederberg *et al.*, 2001), and reduces the embryo's ability to mount an antioxidant defense (Ornoy *et al.*, 1999). Moreover, the teratogenic mechanism is linked to reduced catalase activity, altered metabolism of inositol and arachidonic acid, decreased prostaglandin E2 levels, decreased

expression of the cyclooxygenase-2 gene, elevated apoptosis, and significant disruptions in cell signaling due to changes in protein kinase C. (Gareskog and Wentzel, 2004).

In the present study, light and electron microscopic assessment of the lumbar and the sacral vertebrae of the alloxan plus arachidonic acid group of all studied age groups showed normal tissue and cell structure as compared to the control group. These findings prove the protective effect of AA against alloxan-induced apoptosis which may be explained based on the anti-diabetic characteristics of arachidonic acid (Das, 2018). The normal blood glucose levels in the alloxan+arachidonic acid group demonstrated that arachidonic acid prevented alloxan-induced diabetes, which supported the role of arachidonic acid in preventing alloxan-induced diabetes. These results corroborated those of other researchers who showed that arachidonic acid inhibits alloxan's apoptotic activity by preventing DNA fragmentation, which preserves the integrity of the β cells and keeps them functional (Gundala *et al.*, 2016). This is consistent with earlier studies that showed arachidonic acid's protective effects against type 1 and type 2 diabetes mellitus (Das, 2018). Arachidonic acid not only stopped the onset of diabetes caused by alloxan but also brought the antioxidant status back to normal (Suresh and Das, 2001). This is a crucial feature for β cells since their capacity to release insulin is critical for preventing diabetes and managing hyperglycemia.

Declarations:

Ethical Statement: All experimental procedures were approved by the Institutional Ethics Committee of the faculty of medicine at Assiut University (Approval No 17200437).

Acknowledgments: This research received support from Faculty of Medicine, Assiut University.

Author contribution: Prf. Dr. Refaat Shehata: Conceptualization, guidance, feedback, and constant encouragement throughout the duration of this research. Prof. Dr. Ayman Salaheldeen: Guidance, revision and advice through all the stages of writing this research. Dr. Ashraf Edward: Guidance and revision of all stages of this research. Dr. Martha Emil: data analysis, investigation, visualization, writing original draft.

Data availability statement: Data related to this research can be obtained from the author based on appropriate request.

Author Disclosure Statement: There is no conflict of interest.

Funding Information: The research did not receive funds.

REFERENCES

Aberg, A., Westbom, L. and Kallen, B. (2001): Congenital malformations among infants whose mothers had gestational diabetes or preexisting diabetes. *Early Human Development,* 61: 85-95.

Balaji, P., Madhanraj, R., Rameshkumar, k., Veeramanikandan, V., Eyini, M., Arun, A., Thulasinathan, B., Al Farraj, D. A., Elshikh, M. S., Alokda, A. M., Mahmoud, A. H. Tack, J. C. and Kim, H. J. (2020): Evaluation of antidiabetic activity of Pleurotus pulmonarius against streptozotocin-nicotinamide induced diabetic wistar albino rats. *Saudi Journal of Biological Sciences,* 27: 913-924.

Bamfo, J. E. A. K. and Odibo, A. O. (2011): Review article: Diagnosis and management of fetal growth restriction. *Journal of Pregnancy,* 2011: 640715.

Burdan, F., Błaszczak-Szalak, M., Różyło-Kalinowska, I., Klepacz, R., Dworzański, W., Różyło, T. K., Dudka, J. and Szumiło, J. (2016): Early postnatal development of the lumbar vertebrae in male Wistar rats: double staining and digital radiological studies. *Folia Morphologica,* 75 (1): 1-13.

Cederberg, J., Basu, S. and Eriksson, U. J. (2001): Increased rate of lipid

peroxidation and protein carbonylation in experimental diabetic pregnancy. *Diabetologia*, 44: 766-774.

Das, U. N. (2018): Arachidonic acid in health and disease with focus on hypertension and diabetes mellitus: A review. *Journal of Advanced Research*, 11: 43-55.

DeSesso, J. M. and Scialli, A. R. (2018): Bone development in laboratory mammals used in developmental toxicity studies. *Birth Defects Research*, 110: 1157-1187.

El-Nahla, S. M. M., El-Mahdy, T. O. M., Takahashi, S. and Basha, W. A. (2017): Effects of dietary soybean phytoestrogens usage on the skeleton of albino rats during in-utero development. *Journal of American Science*, 13 (5): 59-72.

El-Sayyad, H. I. H., El-Ghawet, H. A., Al-Haggar, M. S. and Bakr, I. H. (2015): Impairment of bone growth of wistar rat fetuses of diabetic and hypercholesterolemic mothers. *Egyptian journal of basic and applied sciences*, 2: 1-12.

Eriksson, U. J. and Wentzel, P. (2015): The status of diabetic embryopathy. *Upsala journal of medical sciences*, 121(2): 96-112.

Gareskog, M. and Wentzel, P. (2004): Altered protein kinase C activation associated with rat embryonic dysmorphogenesis. *Pediatric Research*, 56: 849-857.

Guevara-Morales, J. M., Frohbergh, M., Castro-Abril, H., Vaca-González, J. J., Barrera, L. A., Garzón-Alvarado, D. A., Schuchman, E. and Simonaro, C. (2020): Growth plate pathology in the mucopolysaccharidosis type VI rat model an experimental and computational approach. *Diagnostics*, 10 (6): 360.

Gundala, N. K. V., Naidu, V. G. M. and Das, U. N. (2016): Arachidonic acid and lipoxin A4 attenuate alloxan-induced cytotoxicity to RIN5F cells in vitro and type 1 diabetes mellitus in vivo. *BioFactors*, 43 (2): 251-271.

Gundala, N. K. V., Naidu, V. G. M. and Das, U. N. (2018): Amelioration of streptozotocin-induced type 2 diabetes mellitus in Wistar rats by arachidonic acid. *Biochemical and Biophysical Research Communications*,496: 105-113.

Hassanin, H. M. (2018): Histological and morphometric studies on the postnatal development of bones under the effect of hypothyroidism and thyroxin replacement in the albino rats. Thesis for the M. D. degree in human anatomy and embryology. Faculty of Medicine, Assiut University, pp: 101-102.

Jones, T. C., Mohr, U. and Hunt, R. D. (1991): Development of the rat skeleton. In: Cardiovascular and musculoskeletal systems. 1st edition. Springer-Verlag, pp: 173-175.

King, A. J. F. (2012): The use of animal models in diabetes research. *British Journal of Pharmacology*, 166: 877-894.

Kume, S., Kato, S., Yamagishi, S., Inagaki, Y., Ueda, S. and Arima, N. (2005): Advanced glycation end-products attenuate human mesenchymal stem cells and prevent cognate differentiation into adipose tissue, cartilage, and bone. *Journal of Bone and Mineral Research*, 20 (9): 1647-1658.

Maynard, R. L. and Downes, N. (2019): Vertebrae, Ribs, Sternum, Pectoral and Pelvic Girdles, and Bones of the Limbs. In: Anatomy and histology of the laboratory rat in toxicology and

biomedical research. 1st edition. Elsevier, pp: 23-29.

Obeid, R. F., Abdelmoneim, H. S. and Elsharkawy, R. T. (2020): Histological evaluation of the antioxidant effect of vitamin E on reversing the negative impact of Tartrazine on extraction socket healing (randomized controlled trial). *Egyptian Dental Journal*, 66: 285-292.

Ornoy, A., Zaken, V. and Kohen, R. (1999): Role of reactive oxygen species (ROS) in the diabetes-induced anomalies in rat embryos in vitro: reduction in antioxidant enzymes and low-molecular-weight antioxidants (LMWA) may be the causative factor for increased anomalies. *Teratology*, 60: 376-386.

Saleh, M. N. M., Hassan, S. A. S., Mahmoud, F. Y. and Shenouda, M. B. K. (2017): The effect of maternal-induced diabetes on postnatal development of the paraventricular and ventromedial hypothalamic nuclei in albino rats: a histological, immunohisto-chemical, and morphometric study. *Journal of Current Medical Research and Practice, 2*: 47-62.

Shamsi, M. M., Ranjbar, R., Mahabady, M. K., Tabandeh, M. R., Khazaeel, K. and Najafzadeh, H. (2020): Protective Effect of Quercetin on Morphological and Histometrical Changes of Placenta in Streptozotocin-Induced Diabetic Rat. *Zahedan Journal of Research in Medical Sciences*, 22 (1): e88636.

Shanbhogue, V. V., Hansen, S., Frost, M., Jørgensen, N. R., Hermann, A. P. and Henriksen, J. E. (2015): Bone Geometry, Volumetric Density, Microarchitecture, and Estimated Bone Strength Assessed by HR-pQCT in Adult Patients with Type 1 Diabetes Mellitus. *Journal of Bone and Mineral Research*, 30 (12): 2188-99.

Sirasanagandla, S. R., Pai, K. S. R., Potu, B. K. and Bhat, K. M. R. (2014): Protective effect of Cissus quadrangularis Linn. on diabetes induced delayed fetal skeletal ossification. *Journal of Ayurveda & Integrative Medicine*, 5(1): 25-32.

Suresh, Y. and Das, U. N. (2001): Protective action of arachidonic acid against alloxan-induced cytotoxicity and diabetes mellitus. *Prostaglandins, Leukotrienes and Essential Fatty Acids*, 64 (1): 37-52.

Szkudelski, T. (2001): The mechanism of Alloxan and Streptozotocin Action in B Cells of the Rat Pancreas. *Physiological Research*, 50 (6): 537-546.

Tani, S., Chung, U. Ohba, S. and Hojo, H. (2020): Understanding paraxial mesoderm development and sclerotome specification for skeletal repair. *Experimental & molecular medicine*, 52 (8): 1166-1177.

Treuting, P. M., Dintzis, S. M. and Montine, K. S. (2018): Skeletal system. In: Comparative anatomy and histology. Elsevier, pp: 68-88.

Tsur, A., Feldman, B. S., Feldhammer, I., Hoshen, M. B., Leibowitz, G. and Balicer, R. D. (2013): Decreased serum concentrations of 25-hydroxycholecalciferol are associated with increased risk of progression to impaired fasting glucose and diabetes. *Diabetes Care*, 36 (5): 1361-7.

Vinceti, M., Malagoli, C., Rothman, K. J., Rodolfi, R., Astolfi, G. and Calzolari E. (2014): Risk of birth defects associated with maternal pregestational diabetes. *European Journal of Epidemiology*, 29: 411-18.

Xian, C. J., Howarth, G. S., Cool, J. C. and Fostera B. K. (2004): Effects of acute 5-fluorouracil chemotherapy and insulin-like growth factor-I pretreatment on growth plate cartilage and metaphyseal bone in rats. *Bone*, 35: 739-749.

Yang, X., Borg, L. A. and Eriksson, U.J. (1997): Altered metabolism and superoxide generation in neural tissue of rat embryos exposed to high glucose. *American Journal of Physiology*, 272: E173-180.

Yilmaz, S. and Tokpinar, A. (2019): Double staining in rats (mini review). *Scientific and Technical Research, 16* (4): 12282-12285.

Zoetis, T., Tassinari, M.S., Bagi, C., Walthall, K. and Hurtt, M.E. (2003): Species comparison of postnatal bone growth and development. *Birth Defects Research B Developmental and Reproductive Toxicology*, 68: 86-110.